DIRECT DETECTION OF EXOPLANETS IN POLYCHROMATIC LIGHT WITH SELF-COHERENT CAMERA

Johan Mazoyer[1a], Pierre Baudoz[1], Raphaël Gallicher[1], and Gérard Rousset[1]

LESIA-Observatoire de Paris, CNRS, UPMC, Université Paris-Diderot, 5 place Jules Janssen, 92195 Meudon Principal Cedex, France

Abstract. Direct detection of exoplanets is a very promising field in astronomy today. Planets unseen by other methods can be discovered and spectroscopically characterized. However, such detections require to overcome the high contrast (larger than 10 thousands up to several billions) and the high angular resolution (smaller than a fraction of arcsec) between the star and its companion. Coronagraphs are being used to reduce the stellar light but their efficiency is limited by wavefront aberrations that produce speckles in the final coronagraphic science plane. Classical adaptive optics usually measure aberrations in a specific estimation channel. To avoid differential aberrations in separate channels, several methods have been developed to estimate the wavefront deformations directly from the science image. Among them, the Self-Coherent Camera (SCC), which uses the principle of the star light coherence to measure the wavefront after a coronagraph. Associated with a deformable mirror, correction in closed-loop with this method has already reached high contrasts in monochromatic light. However, the widening of the wavelength bandwidth, mandatory for spectroscopic analysis of planets, limits the performance in both the estimation by the SCC and the correction by the deformable mirror. After recalling the SCC principle, we will present a theoretical analysis of this problematic and laboratory performance in polychromatic light.

1 Introduction

The detection of exoplanets is a very promising field in astronomy. Most of the known exoplanets were found using indirect methods, but for the last ten years, planets ([13]) and even planetary systems ([15]) were found using direct imaging. This method allows the spectroscopic analysis of the companion. However, the main limitation of this technique is the high contrast levels between the planet and the host star. Dedicated instruments such as GPI ([14]), SPHERE ([3]) and P1640 ([11]), to be installed respectively at the South-Gemini observatory, at the VLT and at the Palomar observatory, will soon allow the detection of young Jupiter like planets. However, the detection of rocky planets will require contrast levels better than 10^{-10}. Several instruments are planed on the next generation of ground-base telescope such as EPICS [12] on the E-ELT or NFIRAOS/IRIS [16] on the TMT.

Coronagraphs can be used to achieve high contrast levels, such as the four quadrant phase mask (FQPM [21]) and the double zone phase mask (DZPM [18]) coronagraphs. But their performance is limited by phase and amplitude aberrations in the incident wavefront, which produce stellar leakage speckles in the detector plane. To correct for these aberrations, adaptive optics (AO) systems have been developed for ground-based instruments [5,14,11]. But classical AO systems introduce quasi-static non common path aberrations (NCPA) because they use a

---

[a] johan.mazoyer@obspm.fr

dedicated channel for the wavefront sensing: we need to estimate the NCPA directly in the focal plane. For this purpose, techniques have been developed using either the application of several known phase on the DM [4, 9, 22] or a specific instrumental design [10, 23, 19].

Among these, the self-coherent camera (SCC) uses the principle of the star light coherence to spatially encode the speckle and measure the wavefront aberrations directly in the coronagraphic image [1]. Associated with a deformable mirror (DM), active correction in closed loop was demonstrated with this concept in simulation [7] and experimentally [17], in monochromatic light.

In this paper, we present new experimental performance in monochromatic light and first experimental results in polychromatic light.

2 SCC principle

In this section we described quickly the concept of the SCC.

2.1 Speckle field estimation

In a classical coronagraph, after the entrance pupil (of size D_P), we focalize the beam on a coronagraphic mask, which diffracts the on-axis light. In the next pupil plane, a Lyot pupil (of size D_L slightly smaller than D_P) removes this diffracted light. We then focalize the light on the detector. However, aberrations in phase or in amplitude in the incoming wavefront result in speckles in the focal plane (Figure 2, left).

The SCC requires only a small modification of the coronagraph, as shown in Figure 1. In the Lyot stop plane of a coronagraph, we add a small pupil (of size D_R, smaller than D_L) at a distance ξ_0 of the Lyot pupil, which we will call the reference pupil (Figure 1, right).
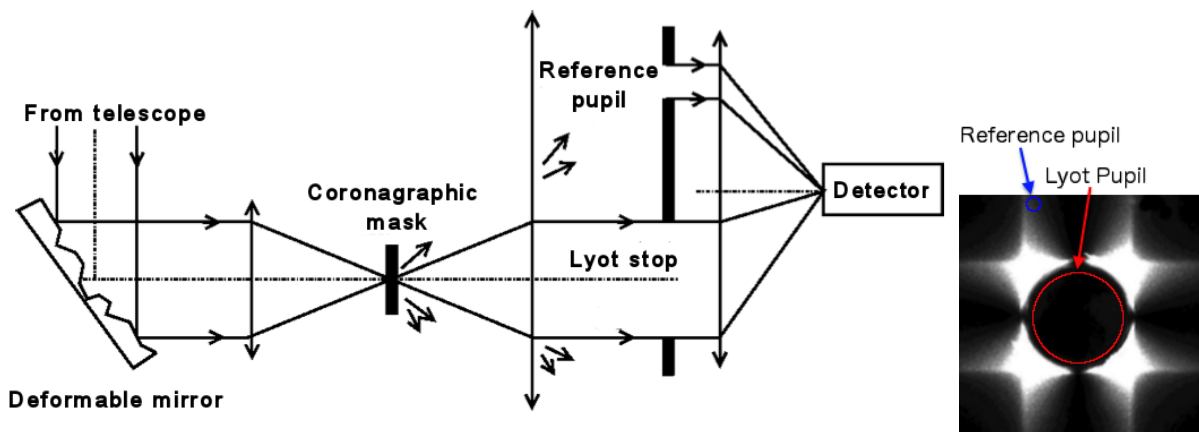

Fig. 1. Principle of the SCC associated with a coronagraph and a DM (left). On the right, light distribution of a four quadrant phase mask (FQPM) coronagraph in the Lyot plane, with the position of the Lyot pupil (red) and reference pupil (blue).

The addition of this pupil will create fringes in the focal plane as shown in Figure 2 (center). If we note A_S (respectively A_R) the complex amplitude in the focal plane of the speckles

(respectively of the reference pupil), the intensity in the focal plane at the wavelength λ_0 reads [7]:

$$I(\alpha, \lambda_0) = |A_S(\alpha, \lambda_0)|^2 + |A_R(\alpha, \lambda_0)|^2$$
$$+A_S(\alpha, \lambda_0)A_R^*(\alpha, \lambda_0)\exp\left(\frac{2i\pi\alpha.\xi_0}{\lambda_0}\right) + A_S^*(\alpha, \lambda_0)A_R(\alpha, \lambda_0)\exp\left(-\frac{2i\pi\alpha.\xi_0}{\lambda_0}\right), \tag{1}$$

where α is the coordinate in the focal plane and X^* is the conjugate of X. The two first terms are the intensity of the light going through the Lyot pupil and the reference pupil. The two other terms express the interference between the two pupils. When applying a Fourier transform
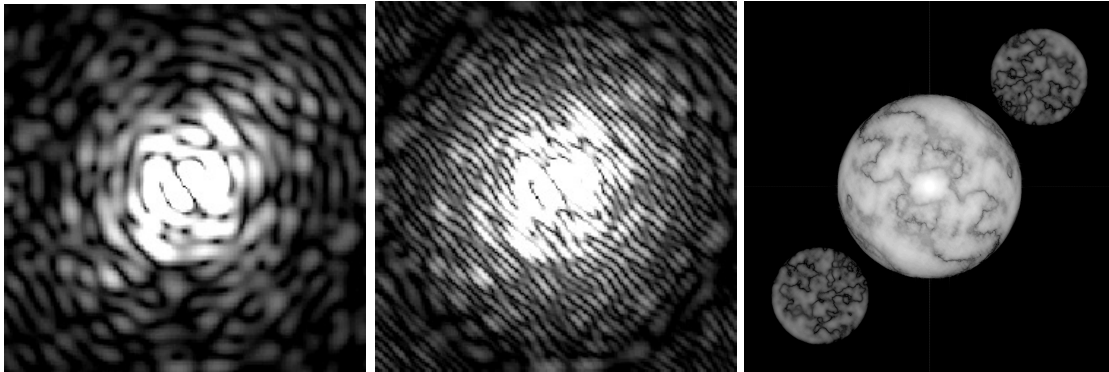

Fig. 2. Simulation of the focal plane of an FQPM coronagraph (left). Simulation of the focal plane of an FQPM coronagraph associated with an SCC (center). Fourier transform of the latter (right).

to this image, we obtain the image presented in Figure 2 (right). With the assumption $\xi_0 > 1.5D_L$ [17], we obtain three distinct peaks. We thus decompose I into a sum of three terms: $I = I_{cent} + I_+ + I_-$. The central peaks is equal to

$$\mathcal{F}[I_{cent}] = \mathcal{F}[|A_S|^2 + |A_R|^2], \tag{2}$$

while we have for the two lateral peaks

$$\mathcal{F}[I_-](\mathbf{u}) = \mathcal{F}[A_S A_R^*](u) * \delta(\mathbf{u} - \xi_0/\lambda_0)$$
$$\mathcal{F}[I_+](\mathbf{u}) = \mathcal{F}[A_S^* A_R](u) * \delta(\mathbf{u} + \xi_0/\lambda_0), \tag{3}$$

where $\mathcal{F}$ is the Fourier transform, $\mathbf{u}$ is the coordinate in the Fourier plane and δ the Kronecker delta). We select one of the lateral peak and apply an inverse Fourier transform. We obtain $I_- = A_S A_R^*$. From this estimate of the complex spectral field, we developed two techniques to correct speckles, using a DM situated in a pupil plane upstream of the coronagraph. The first one use a model of the coronagraph to produce an estimate of the wavefront (phase and amplitude aberrations) in the entrance pupil. Results on an experimental test bench were presented in Mazoyer et al. (2013) [17]. In the second technique, we directly minimize $A_S A_R^*$, the amplitude of the speckles in focal plane, using an interaction matrix. The construction of the interaction matrix is described in the next section.

2.2 Matrix creation and minimization

The interaction matrix links the movements of the actuators (*i.e.* the voltages applied to each actuators) to their effect in the estimate. We choose a base of influence functions to create the

matrix. The response in the estimate plane must be gathered around one point. Indeed, it allows to have to have a high signal to noise ratio (SNR) in this plane with small voltages applied to the actuators. We thus choose to use a base of functions composed of sinus and cosinus as in Poyneer & Véran (2005) [20].
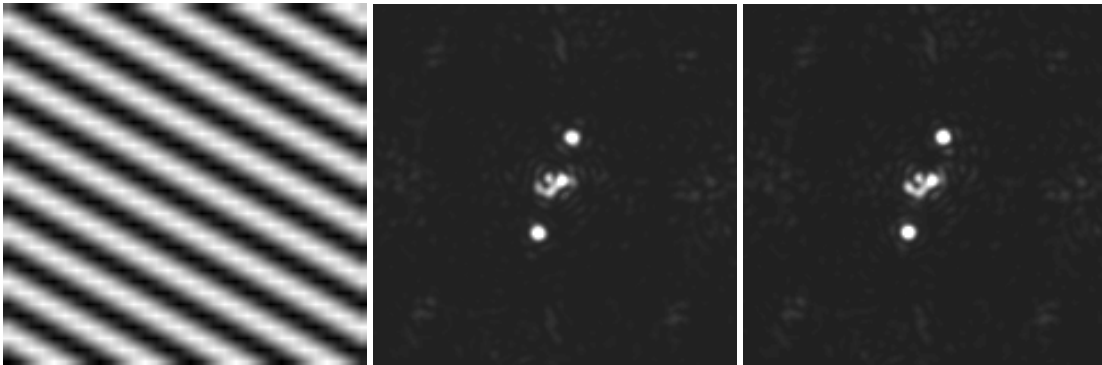

Fig. 3. On the left, the voltage map applied to the 32x32 actuators of the DM to realize one of the cosinus functions on the DM. Each pixel is a voltage to apply to an actuators. We record the images in focal plane of the SCC when we apply to the DM's actuators the vector of tension $V_{ini} + V_{cos}$ (center) and when we apply the vector of tension $V_{ini} - V_{cos}$ (right).

Figure 4 and 3 present experimental images conducted on a optical bench of the creation of a matrix. Starting with a given position of the actuators (*i.e.* vector of voltages) V_{ini}, we apply the vector of tension $V_{ini} - V_{cos}$ and $V_{ini} + V_{cos}$, where V_{cos} is a vector of tension for a cosinus function (*e.g.* the voltage map presented in Figure 4, left). We record the two SCC images $I_{V_{ini}+V_{cos}}$ and $I_{V_{ini}-V_{cos}}$, presented in Figure 4 (center and right). Assuming a linear model, we have:

$$I_{V_{ini}+V_{cos}} - I_{V_{ini}-V_{cos}} = 2I_{V_{cos}}. \tag{4}$$
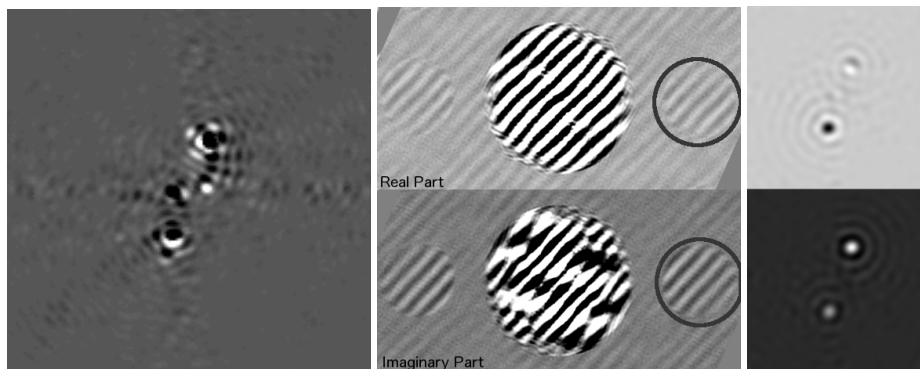

Fig. 4. On the left image, we subtract the two SCC images obtained in Figure 4 (center and right) to limit the influence of other aberrations. We apply a Fourier transform to the difference of the images (center). The real and imaginary part of this Fourier transform are represented here on the left. We isolate the lateral peak ($\mathcal{F}[A_S A_R^*](u) * \delta(\mathbf{u} - \xi_0/\lambda_0)$), center it ($\mathcal{F}[A_S A_R^*](\mathbf{u})$) and apply an inverse Fourier transform ($A_S A_R^*$). The imaginary and real parts of the result of this operation is represented on the right.
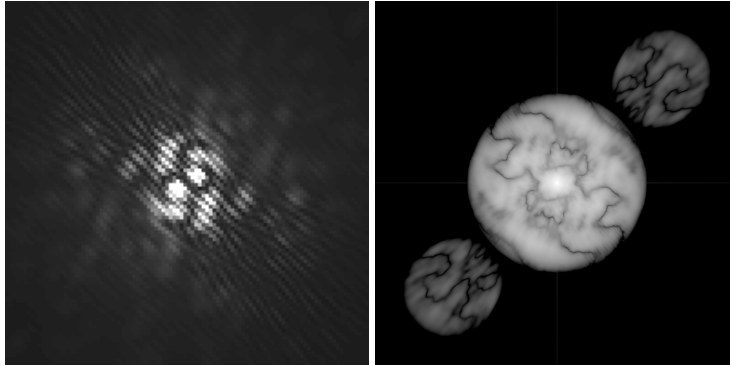
Fig. 5. Simulated speckles field (right) in the focal plane of the SCC in polychromatic light ($r_\lambda = 8$). Due to the multiple wavelengths, the fringes are contrasted in one direction and blurred in the other one. We apply a Fourier transform to this image (right). An other effect of polychromatic light is the deformation of the lateral peaks $\mathcal{I}_-$ and $\mathcal{I}_+$.

Thus, the difference between these two images (Figure 3, left) is assumed to be the response to a perfect cosinus in the estimation plane. We then apply the method described in the previous section: we take the Fourier transform of this difference (Figure 3, center), select the lateral peak and apply a inverse Fourier transform. We obtain the estimated complex speckle field, presented in Figure 3 (real part in top right, imaginary part in bottom right). This estimation is then reform in a 1D vector.

We repeat this operation for all the frequencies achievable by the DM and obtain an interaction matrix, linking the movements of the actuators to their effect in the estimate. This matrix is then inverted using the singular value decomposition method, to obtain the control matrix, which allows us to correct for speckles in the focal plane. Results in monochromatic light are presented in Section 3.2. In the next section we deal with issues in polychromatic light.

2.3 Polychromatic issues

For a larger bandwidth $[\lambda_{min}, \lambda_{max}]$, we define $r_\lambda = \lambda/(\lambda_{max} - \lambda_{min})$ the spectral bandwidth and $\lambda_0 = (\lambda_{max} + \lambda_{min})/2$ the central wavelength. When using the SCC with monochromatic light, the superposition of multiple fringe patterns at different wavelengths (and thus different interfringes) will tend to blur the fringes far away from the null optical path distance (OPD) fringe. Therefore, the focal plane will only be fringed in a stripe of width d_{r_λ}. This limits the estimation and thus the correction of the speckles to a certain zone. This zone is a stripe centered on the null OPD fringe. Assuming a flat spectrum, the width of this fringe can be found in Galicher et al. (2010) [7]:

$$d_{r_\lambda} = \frac{r_\lambda \lambda_0}{2\xi_0}. \tag{5}$$

Figure 5 (left) shows this stripe in a speckles fringes for $r_\lambda = 8$. This limitation can be overcome by the use of a second reference pupil. Indeed, the addition of a second reference pupil at a different angle in the Lyot plane produces an other fringe pattern. It expands the fringed zone and provides a more complete estimate of the complex field in the focal plane. Therefore, it enlarges the correction zone for large bandwidth. A simulation study of the multi-reference SCC including experimental results is presented in Galicher et al. (2013) [8].

5

One can notice that the same effect of superposition of wavelengths also appears in the Fourier plane. The superposition of peaks situated of size $d_{peaks} \in [(D_L + D_R)/\lambda_{max}, (D_L + D_R)/\lambda_{min}]$ and of distance to the center $l_{peaks} \in [\|\xi_0\|/\lambda_{max}, \|\xi_0\|/\lambda_{min}]$. The Fourier transform of a polychromatic SCC image for $r_\lambda = 8$ in shown in Figure 5 (center). In the next section, we present narrow band results.

3 Results

3.1 Bench description

The THD test bench is located in Paris Observatory. We present the main components below:

1. An optical fiber source fed either by a quasi-monochromatic fiber laser diode at 637 nm ($\Delta\lambda < 1$ nm) or by a super-continuum filtered fiber laser source.
2. Two filters to select the central wavelength λ_0 and spectral bandwidth $\delta\lambda$. We can choose between:
    (a) $\lambda_0 = 643.7$ nm and $\Delta\lambda = 9.4$ nm,
    (b) $\lambda_0 = 652.2$ nm and $\Delta\lambda = 35.0$ nm,
3. A tip-tilt mirror and a Boston Micromachines deformable mirror of 32x32 actuators (only 27x27 in the entrance pupil)
4. A coronagraph including:
(a) An FQPM, optimized for the wavelength $\lambda_{opt} = 637$ nm
(b) A Lyot stop with a diameter of 8 mm for an entrance pupil of 8.1 mm
(c) In this same plane a reference pupil of variable size (from 0.3 mm to 2 mm). A set of motors allows to choose between Lyot pupil or the reference pupil only.
5. An sCMOS camera with a readout noise of 1.3 electrons and a full well capacity of 56,000 electrons
6. A set of neutral density filters used to record unsaturated non-coronagraphic images to measure contrast levels.

3.2 Contrasts levels

For both monochromatic light and for narrowband results, we create a matrix using the method described in Section 2.2. We then correct for the speckles in close loop for a few iterations, until we obtain a stable correction. Because we want to correct phase and amplitude defects with only one DM, we limit the correction zone to an half-DH [4]. To measure the achieved contrast inside the DH, we normalize by the maximum of the point spread functions (PSF) obtained without coronagraph. Then we plot the radial profiles of the azimuthal standard deviation (in RMS) of the intensities in the focal plane as a function of the distance to the star (measure in λ/D). We exclude from this measurement the zones located less than 2 λ_0/D away from the FQPM transitions.

For both monochromatic and polychromatic tests, we obtained contrast levels better than 2.10^{-8} between 5 and 12 λ/D. The current limitation are due to the high amplitude defects introduced by the surface of the DM (see [17]). A forthcoming article will describe analyze precisely the performance of the SCC in polychromatic light.
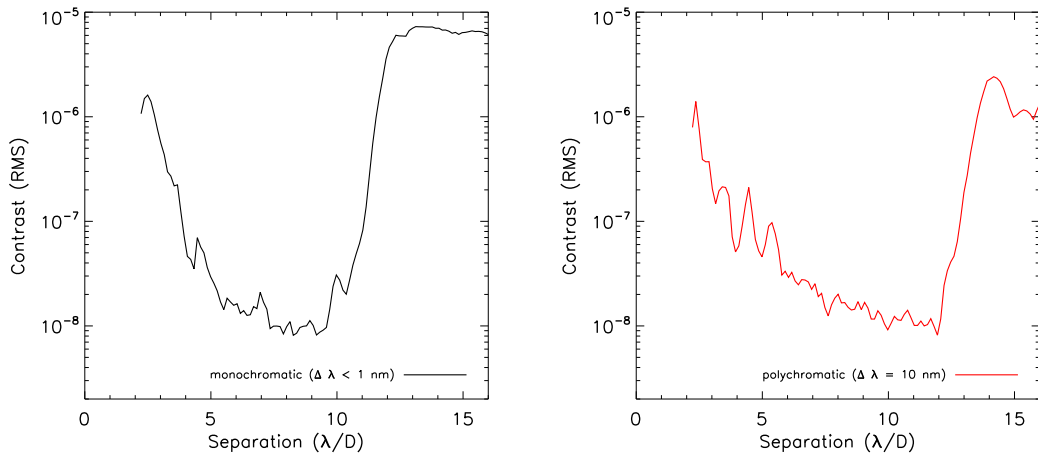
Fig. 6. Radial profiles of the azimuthal standard deviation (in RMS) of the intensities in the focal plane as a function of the distance to the star (measure in λ/D) for monochromatic light (left) and for polychromatic light in narrow band.

4 Conclusion

In this paper, we introduce a new usage of the SCC concept. We also describe the specific issues appearing in the broadening of the bandwidth. We show bench results for monochromatic and polychromatic ($\Delta\lambda = 9.4$ nm) light of the sCC used with a 32x32 actuators DM and a FQPM. We obtained contrast levels better than 2.10^{-8} between 5 and 12 λ/D. This technique shows an improvement of a factor 20 compared to the previous usage [17] of the SCC.

References

1. Baudoz, P., et al., IAU Colloq. 200, (2006) 553
2. Baudoz, P., et al., SPIE, 7736 (2010) 77365S
3. Beuzit, J.-L., et al., SPIE, 7014 (2008) 701418
4. Borde, P. & Traub, W., Astrophysical Journal, 638 (2006) 488
5. Fusco, T. et al., Optics Express, 14, (2006) 7515
6. Galicher, R., et al., Astronomy and Astrophysics, 488, (2008) L9
7. Galicher, R., et al., Astronomy and Astrophysics, 509, (2010) id.A31
8. Galicher, R., et al., A04ELT3 proceedings, (2013)
9. Give'on, A. et al., J. Opt. Soc. Am., 23, (2006) 1063
10. Guyon, O. et al., ApJ, 693, (2009) 75
11. Hinkley, S., et al., PASP, 123, (2011) 74
12. Kasper, M. E. et al in SPIE 7015, (2008)
13. Lagrange, A.-M., et al., Astronomy and Astrophysics, 493, (2009) L21
14. Macintosh, B., et al., SPIE, 7015 (2008) 701518
15. Marois, C. et al., Science, 322, (2008) 1348
16. Marois, C. & Veran, J.-P. in AO4ELT2 (2011) id.27
17. Mazoyer, M., et al., Astronomy and Astrophysics, 557, (2013) id.A9
18. N'diaye et al., Astronomy and Astrophysics, 538, (2012) A55
19. Nishikawa, J., Astronomy and Astrophysics, 489, (2008) 1389

20. Poyneer, L. A. & Véran, J.-P., Journal of the Optical Society of America, A 22, (2005) 1515
21. Rouan, D., et al., PASP, 112, (2000) 1479
22. Sauvage, J.-F. et al., Journal of the Optical Society of America, 24, (2007) 2334
23. Wallace, J. K. et al., SPIE 7736, (2010)